Neural Computing and Applications
https://doi.org/10.1007/s00521-021-06238-6

ORIGINAL ARTICLE

Assessment of critical buckling load of functionally graded plates using artificial neural network modeling

Huan Thanh Duong[1] · Hieu Chi Phan[2] · Tu Minh Tran[3] · Ashutosh Sutra Dhar[4]

Received: 17 October 2020 / Accepted: 13 June 2021

Abstract
Predicting the critical buckling loads of functionally graded material (FGM) plates using an analytical method requires solving complex equations with various modes of deformation to determine the minimum loads. The approach is too complex for application in engineering practice. In this paper, a data-driven model using the artificial neural network (ANN) is proposed for the critical buckling load of FGM plates, as an alternative tool for practicing engineers. A database is first developed for randomly selected inputs using an analytical solution based on first-order shear deformation theory for simply supported FGM plates. The database is then divided into a training dataset with 80% of the data and a testing dataset with 20% of the data for developing and validating, respectively, the ANN model. The ANN model developed using six hidden layers with 32 nodes in each layer is found to match the data with a coefficient of determination of 99.95%. Using the ANN model, the stochastic characteristic of the critical buckling load is examined with respect to randomness of the input parameters. The study reveals that along with the dimensional parameters, the critical buckling load is significantly affected by the randomness of the volume fraction ratio and ratio of the modulus of elasticity of the ceramic and the metal.

Keywords Functionally graded material · Buckling analysis · Shear deformation plate theory · Machine learning · Artificial neural network · Monte Carlo simulation

1 Introduction

Functionally graded materials (FGMs) are advanced materials designed to possess properties varying continuously and smoothly within the structure. Typically, FGMs are composed of metal and ceramic. The ceramic constituent of FGMs provides an excellent heat-resistant property due to its low thermal conductivity, while the ductile metal constituent provides a crack-resistant property. Because of these beneficial properties FGMs are widely used in many engineering applications, such as the structural components in space vehicles, nuclear reactors, and other high thermal applications. However, the behavior of FGMs is very complex, due to the complexity in the manufacturing process and the uncertainties in the properties of the component materials (i.e., metal and ceramic). Understanding the mechanical behavior of FGM structural elements accounting for the uncertainties is very important for the design and maintenance of FGM structures.

Different studies were conducted in the past to develop analytical solutions for the stability of FGM plates and cylindrical shell structures. Zhao et al. [1] used the first-order shear deformation theory (FSDT), in conjunction with the element-free kp-Ritz method, to analyze the mechanical and thermal buckling behavior of FGM plates. An analytical approach (Levy-type solution) based on a higher-order shear deformation theory (HSDT) was proposed by Bodaghi and Saidi [2] for buckling analysis of

✉ Hieu Chi Phan
phanchihieu@lqdtu.edu.vn

[1] Faculty of Engineering, Vietnam National University of Agriculture, Trau Quy, Gia Lam, Hanoi 100000, Vietnam

[2] Lecturer, Institute of Techniques for Special Engineering, Le Quy Don Technical University, 236 Hoang Quoc Viet, Hanoi 100000, Vietnam

[3] Faculty of Building and Industrial Construction, National University of Civil Engineering, 55 Giai Phong, Hanoi 100000, Vietnam

[4] Faculty of Engineering and Applied Science, Memorial University of Newfoundland, St. John's, NL A1B 3X5, Canada

Published online: 03 July 2021

thick FGM rectangular plates. Shariat and Eslami [3] used the third-order shear deformation theory (TSDT) to study the buckling of thick rectangular FGM plates under mechanical and thermal loads. Thai and Choi [4, 5] also employed the TSDT for buckling analysis of FGM plates. In these studies, governing equations were derived from the principle of minimum total potential energy, and closed-form solutions of rectangular plates were obtained. Thai and his colleagues [6, 7] used two variable refined plate theories and a new sinusoidal shear deformation theory for bending, buckling, and vibration analyses of thick rectangular plates with various boundary conditions. Nguyen et al. [8] obtained Navier-type solutions for simply supported FGM sandwich plates for vibration and buckling analysis based on the FSDT. Tung and Duc [9] presented a simple analytical approach, using the classical plate theory (CPT) to investigate the stability of FGM plates under in-plane compressive, thermal, and combined loads. Huan et al. [10] and Tran et al. [11] used analytical solutions based on the FSDT for analyzing bending, buckling, and vibration of an FGM cylindrical panel. Based on the new eight-unknown HSDT, Thinh et al. [12], Tu et al. [13], and Long et al. [14] studied the bending, buckling and free vibration of FGM plates by analytical and finite element methods. The solutions for the critical buckling loads from the analytical methods are often complex [15] and require trials to solve equations for determining various buckling loads and corresponding buckling modes to obtain the minimum loads. This can be more complex for multi-layered plates with varying material properties. Besides, intrinsic uncertainties in the material properties of FGMs resulting from the complicated manufacturing process often necessitate a non-deterministic/stochastic assessment of the structural behavior [16]. Stochastic analysis using the analytical solution is computationally infeasible. To overcome the challenges of the analytical methods, a data-driven model using an Artificial Neural Network (ANN) is proposed in the current study. The developed model is used for the assessment of a critical buckling load considering the randomness of material properties.

The method of ANN was first introduced in the 1940s by McCulloch and Pitts [17], but was not extensively developed until the late 1980s due to the limitations in computational ability. Nowadays, the ANN is widely used to deal with complex problems, including convolutional networks for image recognition [18], restricted Boltzmann machines [19], deep belief net [20], auto-encoders [21] and others. The applications of ANN for solving engineering problems are gaining interest with various studies such as [22–25] and [23, 24, 26]. In the area of FGM, Ootao et al. [27] applied ANN with the incorporation of optimization to predict the maximum thermal stress in an FGM circular cylinder. Liu et al. [28] applied a modified hybrid numerical method with ANN to predict the dynamic displacement of FGM plates. Jodaei et al. [29] employed ANN for free vibration analysis of FGM plates. To predict the material property of the FGM cylinder, an ANN is implemented with the displacements on the outer surface, are the inputs in Han and Liu [30]. Nazari et al. [31] used a database of 144 experimental results with ANN to predict the temperature corresponding to the ductile/brittle transition for functionally graded steels. However, to the best of the authors' knowledge, the ANN method has not been applied for assessing the stochastic characteristics of the buckling loads on FGM plates. An ANN-based model could be used for studying the stochastic characteristics of buckling loads, as the analytical or numerical models are computationally prohibitive for the task.

In this paper, an ANN model is proposed to estimate the buckling load of biaxial simply supported rectangular plates under various loading conditions with plate dimensions and material properties as the input variables. The ANN method was found to be superior to other machine learning models considered. An analytical method based on first-order shear deformation theory (FSDT) for a simply supported plate is considered for the development of a database. Nondimensional buckling loads are calculated using the analytical method for various randomly generated input variables. The developed ANN model is validated with results from the analytical models for a range of input variables. The ANN model is then applied to assess the stochastic characteristics of the critical buckling load under the influence of the variation of inputs.

2 Theoretical formulation

2.1 Analytical model

An analytical model developed in Thai and Choi [4] is used in this study for the assessment of the critical buckling load. A rectangular plate of length '*a*,' width '*b*,' and total thickness '*h*' as shown in Fig. 1 is considered. The plate is

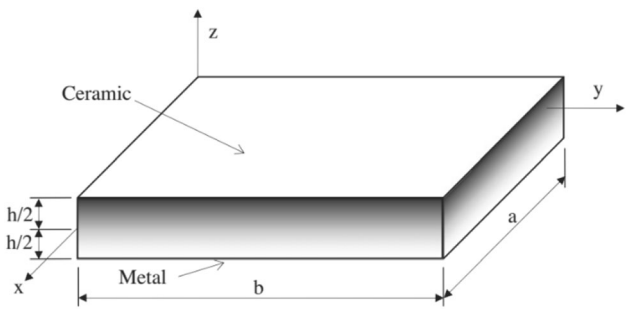

Fig. 1 Geometry and coordinate system of FGM plate

made of isotropic material with material properties varying smoothly along the thickness direction.

The Young's modulus, E, is assumed to vary through the thickness according to a power law, as shown in Eq. (1) [32]:

$$E(z) = (E_c - E_m).\left(\frac{1}{2} + \frac{z}{h}\right)^p + E_m \tag{1}$$

where E_c and E_m are the Young's modulus of the ceramic and metal, respectively, p is the volume fraction exponent ($p \geq 0$), and z is the coordinate in the thickness direction. In this study, the Poisson's ratio, υ, is assumed to be a constant.

According to the first-order shear deformation theory, the displacement field can be expressed as in Eq. (2) [32]:

$$\begin{aligned} u(x,y,z) &= u_0(x,y) + z\phi_x(x,y) \\ v(x,y,z) &= v_0(x,y) + z\phi_y(x,y) \\ w(x,y,z) &= w_0(x,y) \end{aligned} \tag{2}$$

where u_0, v_0 and w_0 denote the displacements at the mid-plane of the plate along the x-, y-, and z-directions. ϕ_x and ϕ_y represent the transverse normal rotations about the y- and x-axes, respectively.

The linear strain–displacement relationship is given by (Eq. 3):

$$\begin{Bmatrix} \varepsilon_x \\ \varepsilon_y \\ \gamma_{xy} \end{Bmatrix} = \begin{Bmatrix} \varepsilon_x^0 \\ \varepsilon_y^0 \\ \gamma_{xy}^0 \end{Bmatrix} + z\begin{Bmatrix} k_x \\ k_y \\ k_{xy} \end{Bmatrix}; \begin{Bmatrix} \gamma_{yz} \\ \gamma_{xz} \end{Bmatrix} = \begin{Bmatrix} \gamma_{yz}^0 \\ \gamma_{xz}^0 \end{Bmatrix} \tag{3}$$

in which

$$\begin{cases} \varepsilon_x^0 = \dfrac{\partial u_0}{\partial x} \\ \varepsilon_y^0 = \dfrac{\partial v_0}{\partial y} \\ \gamma_{xy}^0 = \dfrac{\partial v_0}{\partial x} + \dfrac{\partial u_0}{\partial y} \end{cases} \begin{cases} k_x = \dfrac{\partial \phi_x}{\partial x} \\ k_y = \dfrac{\partial \phi_y}{\partial y} \\ k_{xy} = \dfrac{\partial \phi_y}{\partial x} + \dfrac{\partial \phi_x}{\partial y} \end{cases} \tag{4}$$

$$\begin{cases} \gamma_{yz}^0 = \dfrac{\partial w_0}{\partial y} + \dfrac{\partial v_0}{\partial z} = \dfrac{\partial w_0}{\partial y} + \phi_y \\ \gamma_{xz}^0 = \dfrac{\partial w_0}{\partial x} + \dfrac{\partial u_0}{\partial z} = \dfrac{\partial w_0}{\partial x} + \phi_x \end{cases}$$

The linear constitutive relations of a FGM plate can be written as (Eq. 5):

$$\begin{aligned} \begin{Bmatrix} \sigma_x \\ \sigma_y \\ \sigma_{xy} \end{Bmatrix} &= \begin{bmatrix} Q_{11} & Q_{12} & 0 \\ Q_{12} & Q_{22} & 0 \\ 0 & 0 & Q_{66} \end{bmatrix} \cdot \begin{Bmatrix} \varepsilon_x \\ \varepsilon_y \\ \gamma_{xy} \end{Bmatrix}; \begin{Bmatrix} \sigma_{yz} \\ \sigma_{xz} \end{Bmatrix} \\ &= \begin{bmatrix} Q_{44} & 0 \\ 0 & Q_{55} \end{bmatrix} \cdot \begin{Bmatrix} \gamma_{yz} \\ \gamma_{xy} \end{Bmatrix} \end{aligned} \tag{5}$$

where the coefficients Q_{ij} are determined as:

$$\begin{aligned} Q_{11} = Q_{22} &= \frac{E(z)}{1-\upsilon^2};\ Q_{12} = Q_{21} = \frac{\upsilon E(z)}{1-\upsilon^2};\ Q_{44} = Q_{55} \\ &= Q_{66} = \frac{E(z)}{2(1+\upsilon)} \end{aligned} \tag{6}$$

The total in-plane force resultants, total moment resultants, and transverse force resultants are defined as in Eq. (7).

$$\begin{aligned} \begin{bmatrix} N_x \\ N_y \\ N_{xy} \end{bmatrix} &= \int_{-h/2}^{h/2} \begin{Bmatrix} \sigma_x \\ \sigma_y \\ \tau_{xy} \end{Bmatrix} dz; \begin{bmatrix} M_x \\ M_y \\ M_{xy} \end{bmatrix} \\ &= \int_{-h/2}^{h/2} \begin{Bmatrix} \sigma_x \\ \sigma_y \\ \tau_{xy} \end{Bmatrix} z dz; \begin{bmatrix} Q_x \\ Q_y \end{bmatrix} = \int_{-h/2}^{h/2} \begin{bmatrix} \tau_{xz} \\ \tau_{yz} \end{bmatrix} dz \end{aligned} \tag{7}$$

Substituting Eq. (5) into Eq. (7) and integrating through the thickness of the plate, the stress resultants are given as in Eq. (8).

$$\begin{aligned} \begin{Bmatrix} N_x \\ N_y \\ N_{xy} \end{Bmatrix} &= \begin{bmatrix} A_{11} & A_{12} & 0 \\ A_{12} & A_{22} & 0 \\ 0 & 0 & A_{66} \end{bmatrix} \begin{Bmatrix} \varepsilon_x^0 \\ \varepsilon_y^0 \\ \gamma_{xy}^0 \end{Bmatrix} \\ &+ \begin{bmatrix} B_{11} & B_{12} & 0 \\ B_{12} & B_{22} & 0 \\ 0 & 0 & B_{66} \end{bmatrix} \begin{Bmatrix} k_x \\ k_y \\ k_{xy} \end{Bmatrix} \end{aligned} \tag{8a}$$

$$\begin{aligned} \begin{Bmatrix} M_x \\ M_y \\ M_{xy} \end{Bmatrix} &= \begin{bmatrix} B_{11} & B_{12} & 0 \\ B_{12} & B_{22} & 0 \\ 0 & 0 & B_{66} \end{bmatrix} \begin{Bmatrix} \varepsilon_x^0 \\ \varepsilon_y^0 \\ \gamma_{xy}^0 \end{Bmatrix} \\ &+ \begin{bmatrix} D_{11} & D_{12} & 0 \\ D_{12} & D_{22} & 0 \\ 0 & 0 & D_{66} \end{bmatrix} \begin{Bmatrix} k_x \\ k_y \\ k_{xy} \end{Bmatrix} \end{aligned} \tag{8b}$$

$$\begin{bmatrix} Q_x \\ Q_y \end{bmatrix} = K_s . \begin{bmatrix} A_{44} & 0 \\ 0 & A_{55} \end{bmatrix} \begin{Bmatrix} \gamma_{yz}^0 \\ \gamma_{xz}^0 \end{Bmatrix} \tag{8c}$$

where

$$\begin{aligned} A_{ij} &= \int_{-h/2}^{h/2} Q_{ij} \mathrm{d}z;\ B_{ij} = \int_{-h/2}^{h/2} Q_{ij} z dz;\ D_{ij} \\ &= \int_{-h/2}^{h/2} Q_{ij} z^2 dz;\ \text{with}\ (i;j) = (1,\ 2,\ 4,\ 5,\ 6) \end{aligned} \tag{8d}$$

K_s denotes the transverse shear correction factor (K_s = 5/6, [33–35]).

Using the principle of minimum total potential energy, the governing equations can be obtained as follows [36]:

$$\frac{\partial N_x}{\partial x}+\frac{\partial N_{xy}}{\partial y}=0 \tag{9a}$$

$$\frac{\partial N_{xy}}{\partial x}+\frac{\partial N_y}{\partial y}=0 \tag{9b}$$

$$\frac{\partial Q_x}{\partial x}+\frac{\partial Q_y}{\partial y}-\mathbb{N}(w_0)=0 \tag{9c}$$

$$\frac{\partial M_x}{\partial x}+\frac{\partial M_{xy}}{\partial y}-Q_x=0 \tag{9d}$$

$$\frac{\partial M_{xy}}{\partial x}+\frac{\partial M_y}{\partial y}-Q_y=0 \tag{9e}$$

$$\text{where } \mathbb{N}(w_0)=\widehat{N}_x^0\frac{\partial^2 w_0}{\partial x^2}+\widehat{N}_y^0\frac{\partial^2 w_0}{\partial y^2}+2\widehat{N}_{xy}^0\frac{\partial^2 w_0}{\partial x\partial y} \tag{9f}$$

with $\widehat{N}_x^0$, $\widehat{N}_y^0$, $\widehat{N}_{xy}^0$, the in-plane pre-buckling forces.

Now, consider that the simply supported rectangular plate is subjected to in-plane loading in two directions, such as $\widehat{N}_x^0=N^0$ along the x-axis, $\widehat{N}_y^0=kN^0$ along the y-axis, where k is the load ratio. Based on the Navier method, the following expansions of displacements (u_0, v_0, w_0, ϕ_x, ϕ_y) are obtained to satisfy the simply supported boundary conditions [32]:

$$\begin{aligned}
u_0(x,y)&=\sum_{n=1}^{\infty}\sum_{m=1}^{\infty}u_{mn}\cos\alpha x\sin\beta y;\\
v_0(x,y)&=\sum_{n=1}^{\infty}\sum_{m=1}^{\infty}v_{mn}\sin\alpha x\cos\beta y\\
w_0(x,y)&=\sum_{n=1}^{\infty}\sum_{m=1}^{\infty}w_{mn}\sin\alpha x\sin\beta y;\\
\phi_x(x,y)&=\sum_{n=1}^{\infty}\sum_{m=1}^{\infty}\phi_{xmn}\cos\alpha x\sin\beta y\\
\phi_y(x,y)&=\sum_{n=1}^{\infty}\sum_{m=1}^{\infty}\phi_{ymn}\sin\alpha x\cos\beta y
\end{aligned} \tag{10}$$

where $\alpha=m\pi/a$, $\beta=n\pi/b$.

Substituting Eq. (10) into Eq. (9a), we obtain a 5 × 5 system of the following equations:

$$\begin{bmatrix}
k_{11} & k_{12} & 0 & k_{14} & k_{15}\\
k_{12} & k_{22} & 0 & k_{24} & k_{25}\\
0 & 0 & k_{33}+\widehat{k}_{33} & k_{34} & k_{35}\\
k_{14} & k_{24} & k_{34} & k_{44} & k_{45}\\
k_{15} & k_{25} & k_{35} & k_{45} & k_{55}
\end{bmatrix}
\begin{Bmatrix}
u_{mn}\\ v_{mn}\\ w_{mn}\\ \phi_{xmn}\\ \phi_{ymn}
\end{Bmatrix}=
\begin{Bmatrix}
0\\0\\0\\0\\0
\end{Bmatrix} \tag{11a}$$

in which the coefficients of k_{ij}, m_{ij} are defined as follows:

$$\begin{aligned}
k_{11}&=\left(A_{11}\alpha^2+A_{66}\beta^2\right) & k_{33}&=\left(A_{55}\alpha^2+A_{44}\beta^2\right)K_s\\
k_{12}&=(A_{12}+A_{66})\alpha\beta & \widehat{k}_{33}&=N^0\alpha^2+k\beta^2N^0\\
k_{14}&=\left(B_{11}\alpha^2+B_{66}\beta^2\right) & k_{34}&=A_{55}\alpha K_s\\
k_{15}&=(B_{12}+B_{66})\alpha\beta & k_{35}&=A_{44}\beta K_s\\
k_{22}&=\left(A_{66}\alpha^2+A_{22}\beta^2\right) & k_{44}&=\left(A_{55}K_s+D_{11}\alpha^2+D_{66}\beta^2\right)\\
k_{24}&=(B_{12}+B_{66})\alpha\beta & k_{45}&=(D_{12}+D_{66})\alpha\beta\\
k_{25}&=\left(B_{66}\alpha^2+B_{22}\beta^2\right) & k_{55}&=\left(A_{44}K+D_{66}\alpha^2+D_{22}\beta^2\right)
\end{aligned} \tag{11b}$$

For a nontrivial solution, the determinant of the coefficient matrix in Eq. (11a) must be zero.

$$\begin{vmatrix}
k_{11} & k_{12} & 0 & k_{14} & k_{15}\\
k_{12} & k_{22} & 0 & k_{24} & k_{25}\\
0 & 0 & k_{33}+\widehat{k}_{33} & k_{34} & k_{35}\\
k_{14} & k_{24} & k_{34} & k_{44} & k_{45}\\
k_{15} & k_{25} & k_{35} & k_{45} & k_{55}
\end{vmatrix}=0 \tag{12}$$

Solving Eq. (12), the buckling loads $N_{(m,n)}^0$ corresponding to buckling modes (m, n) can be obtained.

Note that when k = 0, the FGM plate is subjected to uniaxial compression along the x-axis, and when k = 1, the FGM plate is subjected to biaxial compression with equal magnitudes of loads.

The critical buckling load (N_{cr}) is the smallest value of $N_{(m,n)}^0$.

$$N_{cr}=\min\left\{N_{(m,n)}^0\right\} \tag{13}$$

The smallest value of $N_{(m,n)}^0$ is obtained using trials and errors with varying 'm' and 'n.' For the study presented in this paper, the nondimensional critical buckling load of the FGM plate is defined in the following form (Eq. 14) [4].

$$\overline{N}_{cr}=N_{cr}a^2/\left(E_mh^3\right) \tag{14}$$

2.2 ANN model development

Several supervised machine learning models such as random forest regression, extreme gradient boosting, support vector machine, and ANN are first examined and demonstrate the ANN as the most suitable method for the critical buckling load of FGM (discussed later in the paper). Like the other supervised machine learning models, ANN aims to provide a prediction on the variable of interest based on a labeled database. The objective of the training or model developing process is to minimize the difference between actual value y and predicted value $\bar{y}$ of the output corresponding to the ith input x_i through minimizing the loss function Q.

A conventional feedforward ANN with 's' layers for the regression problem with a dataset containing 'r' features (e.g., number of inputs) is shown in Fig. 2. Each node (a neuron) in a layer of the network is connected with all

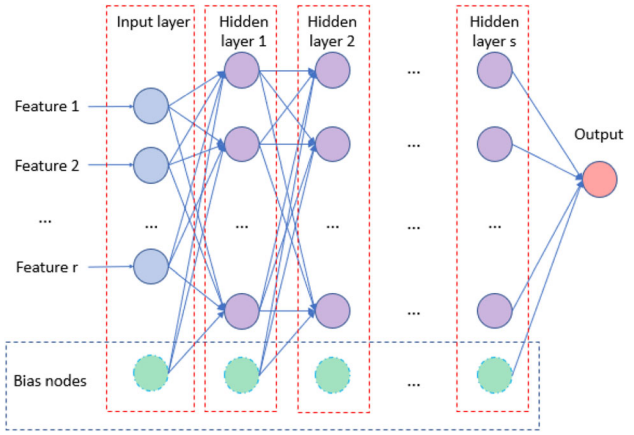

Fig. 2 Example of a feedforward ANN with '*r*' input features and '*s*' hidden layers (adapted from [38])

nodes in the previous and the next layers (i.e., fully connected). With an activation function (e.g., ReLu, sigmoid or Hyperbolic tangent), this neuron generates a signal to the nodes in the next layer until the output layer is reached. A bias node is added to each hidden layer to move the activation function forward or backward. The network is trained by feeding data to the input layer. Each node in this layer takes its corresponding feature for each sample. Every neuron combines its input signals from nodes in the previous layer by a weighted summation. After being fed with the total number of samples (also called the batch size), the loss function in Eq. 15 is calculated. The back-propagation algorithm [37] is implemented to compute the gradient of weights with respect to the loss function. The weights in ANN are thus adjusted based on total samples to update the weights for neuron-to-neuron connections. The weight updating process continues from the first batch to the last batch of the database to finish an epoch. There are a number of epochs to finish the training process for an ANN. There is no strict rule for choosing the batch size and number of epochs required in the training process.

To predict the buckling load, a fully connected ANN is established through trying various configurations of the networks. Five input variables ($r = 5$) for the model include the ratio of in-plane forces corresponding along x- and y-directions (k), volume fraction exponent (p), thickness ratio (b/h), aspects ratio (a/b) and the ratio E_c/E_m. Unlabeled data of random inputs are first generated. The database is then labeled with corresponding $\overline{N}_{cr}$, determined from the analytical method. The labeled database is split into a training dataset and a testing dataset. The training dataset is used for training the ANN while the testing dataset is applied for validation. Figure 3 demonstrates the ANN model development process. The training and validating processes for the ANN model are conducted developing a computer code in the Python programming language.

3 Results

3.1 ANN model

Table 1 shows the ranges of input variables considered for the supervised machine learning model development. The ranges are chosen to develop the ANN model for a wide range of magnitudes of the critical buckling load. The ratio (k) of in-plane forces along x-direction to those along y-direction is randomly generated between -1 and 5. A negative lower bound value indicates a tensile load along one axis and compression along the other axis. The material-related variables, such as the volume fraction exponent 'p' and the ratio E_c/E_m, are assumed to range between [0:10] and [1:10], respectively. The thickness ratio (b/h) and aspects ratio (a/b) are assumed to range between [20:100] and [1:5], respectively. Within these ranges, 4487 set samples of input variables are generated. Then, the analytical method (based on the FSDT) is applied to obtain $\overline{N}_{cr}$ for each set of samples of input variables, which are used to label the input samples. The resulting distribution of $\overline{N}_{cr}$ is shown in Fig. 4. The magnitudes of the load ($\overline{N}_{cr}$) range between [0.67, 364.50], indicating a heavy right-skewed distribution with a mean of 28.0 and a median of 13.30.

The overall database is split into training and testing datasets with a ratio of 4:1. With the training data sets, various ANN configurations are tried along with batch sizes and maximum numbers of the epoch. A model with 6 hidden layers and $32 + 1$ (bias) nodes in each layer is found to reasonably simulate the buckling load. This model involves a total of 206 nodes and 5537 trainable weights and is trained with 10^5 epochs and batches of 500 samples.

A set of metrics is used in this study to validate the developed model on the train and test set, including Coefficient of determination, R^2, Mean absolute error, MAE, and Mean squared error, MSE, in Eqs. 15, 16 and 17, respectively.

$$R^2 = 1 - \frac{\sum_{i=1}^{n}(y_i - f_i)^2}{\sum_{i=1}^{n}(y_i - \overline{y})^2} \tag{15}$$

$$\text{MAE} = \frac{1}{n} \times \sum_{i=1}^{n} |y_i - f_i| \tag{16}$$

$$\text{MSE} = \frac{1}{n}\sum_{i=1}^{n}(y_i - f_i)^2 \tag{17}$$

The training process is conducted with 10^5 iterative steps of updating the weights for the connection between neurons through comparing the model errors (i.e., the loss function). The loss function during the training process against the number of epochs is plotted in Fig. 5. It shows

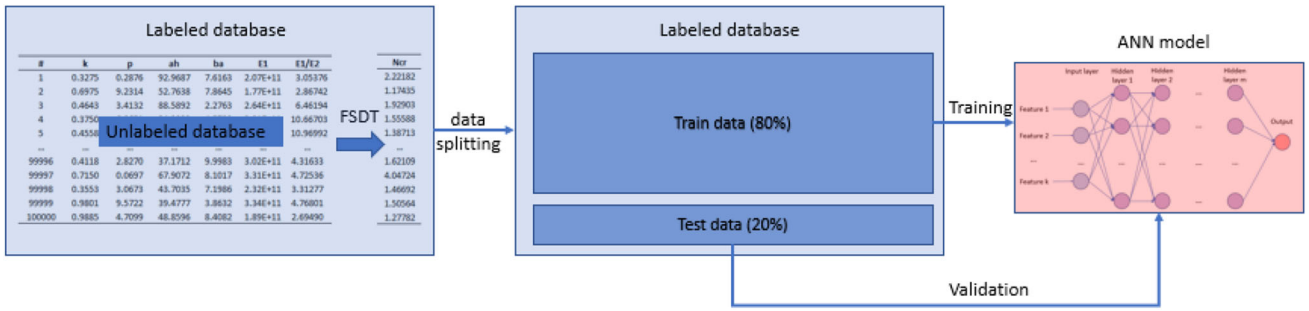

Fig. 3 Scheme of developing ANN model

Table 1 Input parameter ranges for machine learning models

Input	Range
K	[− 1:5]
P	[0:10]
b/h	[20:100]
a/b	[1:5]
E_c/E_m	[1:10]

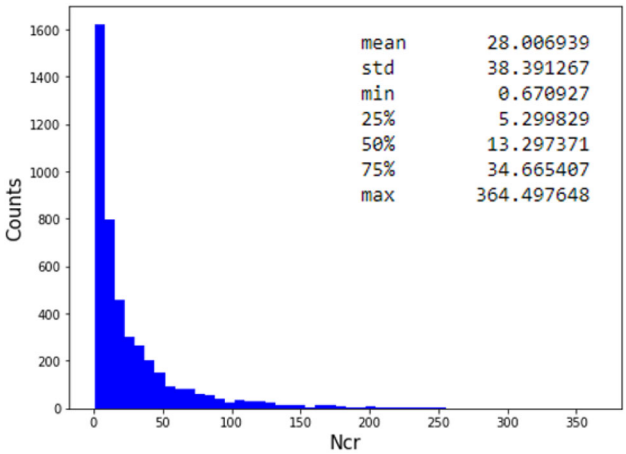

Fig. 4 Histogram and descriptive summary of $\overline{N}_{cr}$ in the database

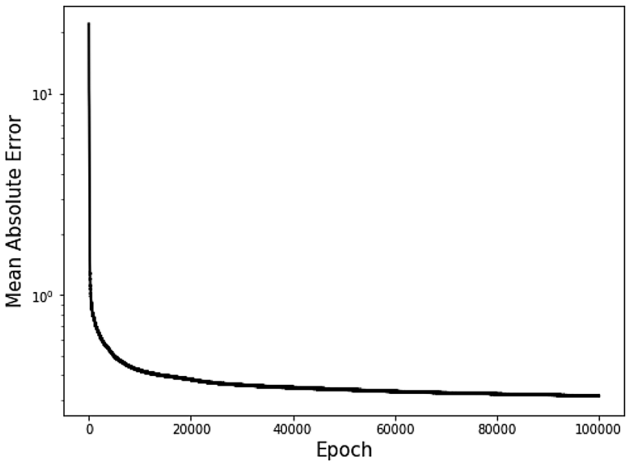

Fig. 5 Error versus number of epochs during the training process

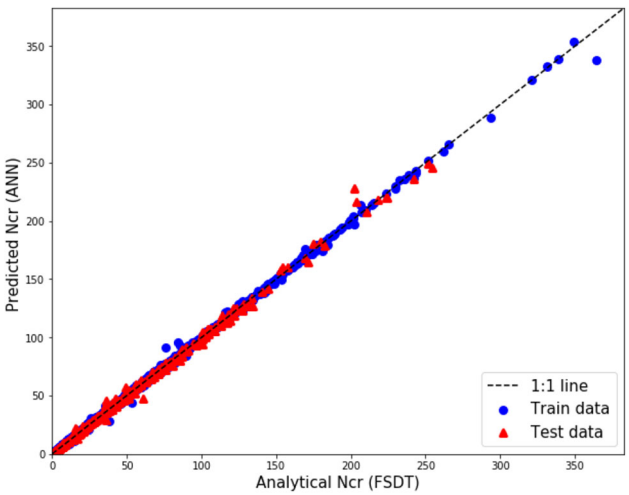

Fig. 6 Scatter plot of analytical $\overline{N}_{cr}$ with FSDT versus predicted $\overline{N}_{cr}$ with ANN

that for the first thousand epochs, the Mean Absolute Error (MAE) dramatically drops from 22.05 to 1.81. For the rest of the training process, MAE gradually decreases from 1.81 to 0.31 along with the improvement of the model.

In a scatter plot in Fig. 6, the $\overline{N}_{cr}$ predicted using the ANN models are compared with those from the analytical solutions. The figure shows the data points concentrating narrowly around the 1:1 line, implying that the predictions using the ANN model match well with the predictions from the analytical model. Table 2 shows the calculated errors of the models. The ANN has the lowest Mean Absolute Error in Table 2 for both training and testing datasets compared to other machine learning models. The ANN model is therefore proposed for the critical buckling load of an FGM plate. For the ANN model, the errors for both testing and training datasets are very low (0.6296 and 0.3135, respectively) with a very high coefficient of determination or R-square value (close to 100%). Given that the developed model fits very well with the data, no further study has been conducted to modify the ANN architecture.

Table 2 Evaluation metrics for ANN model and other machine learning models

Model	Validate on	R^2	MAE	MSE
ANN	Train set	1.0000	0.3135	0.8135
	Test set	0.9981	0.6296	2.7699
Random forest [39, 40]	Train set	0.9939	1.1688	9.4431
	Test set	0.9624	2.7073	45.9287
Xgboost [41]	Train set	0.9995	0.5471	0.7233
	Test set	0.9579	3.1078	60.6407
Support vector machine [42–44]	Train set	0.7109	9.8643	444.0426
	Test set	0.7049	9.3992	360.1878

The benefits of using the ANN model instead of the conventional analytical and numerical models are examined through simulation of the critical buckling load of FGM plates. The analytical method involves solving $\det(K) = 0$, corresponding to each buckling mode, to identify the critical load. This process requires iteration due to the uncertainties of the parameters 'm' and 'n' in Eqs. 13 and 14. For numerical modeling using the finite element method, the computational time is significantly increased with the use of fine mesh, required to obtain accurate solutions. However, an ANN model developed with optimization of the weight factors through the training process can provide simplified solutions. The ANN model is particularly essential for reliability analysis requiring millions of simulations using the Monte Carlo method. Reliability assessments were performed using various methods considering all inputs as normally distributed random variables. Using a computer with a Core i5-8250U processor and 8.00 GB RAM, the analyses took 4.128 h, 711 h, and 774 h for the ANN, analytical, and FEA models, respectively. Thus, the complexity of the problems and the computational time can be significantly reduced using the proposed ANN model.

3.2 Parametric study

The $\overline{N}_{\mathrm{cr}}$ is examined against each of the input variables independently to visualize the effect of input parameters on the buckling load. To examine this, a control case is set with each of the variables varying within the ranges provided in Table 1, while the other variables are set to constant values as: $E_c = 380 \times 10^9$ Pa; $E_m = 70 \times 10^9$ Pa; $\nu = 0.3$; $p = 2$; $b/h = 20$; $a/b = 2$; $k = 1$. Figure 7 plots the variation of $\overline{N}_{\mathrm{cr}}$ against various input parameters. Note that the results obtained from the proposed ANN model match very well with the results from the analytical model in Fig. 7, validating the developed model.

Figure 7a shows that the buckling load significantly changes with the changes in the magnitudes of k. For negative magnitudes of k, the buckling load increases with decreasing magnitudes of k to the maximum value at $k = -0.5$ and then decreases. The buckling load continues to decrease with the increase in the positive magnitude of k. This implies that the critical buckling load (under compression) along one direction can be increased due to a tensile load along the orthogonal direction for the FGM plates, while a compressive force along the orthogonal direction can reduce the buckling load. However, an excessive tension (beyond 50% of the compression) can lead to the reduction in the critical buckling load. The critical buckling load is found to increase with the increase in a/b and E_c/E_m (Fig. 7b, d) and decreases with the increases of p. The length to thickness ratio, b/h, appears to have an insignificant effect on the critical buckling load, $\overline{N}_{\mathrm{cr}}$.

3.3 Stochastic characteristics of $\overline{N}_{\mathrm{cr}}$

The complex manufacturing process of FGM with ceramic and metal, which have significantly different material properties, leads to uncertainties in the behavior of the structural elements made of FGM. The uncertainties in the critical buckling load of FGM plates are investigated here, considering the randomness of material parameters using Monte Carlo simulations (MCS). The input parameters are assumed to be random variables with known normal distributions. The means for k, p, b/h, a/b and E_c/E_m are randomly selected using the range defined in Table 1, except for k, for which a range [0:1] is chosen to reduce right-skewness of the mean. The tension in the orthogonal direction is typically rare for an FGM plate. The coefficients of variances, CV, corresponding to each mean value of the parameters are selected to be uniformly distributed between [0:0.2]. A database containing 10^3 samples is developed for the assessment of the stochastic characteristics of $\overline{N}_{\mathrm{cr}}$. For each sample,$10^6$ Monte Carlo simulations are performed to calculate $\overline{N}_{\mathrm{cr}}$ using the ANN model. Thus, the mean, standard deviation and coefficient variance of $\overline{N}_{\mathrm{cr}}$ from these 10^6 Monte Carlo simulations are recorded as the output (i.e., labels). For the presentation of data and results, symbols 'σ,' 'CV' and 'μ' are

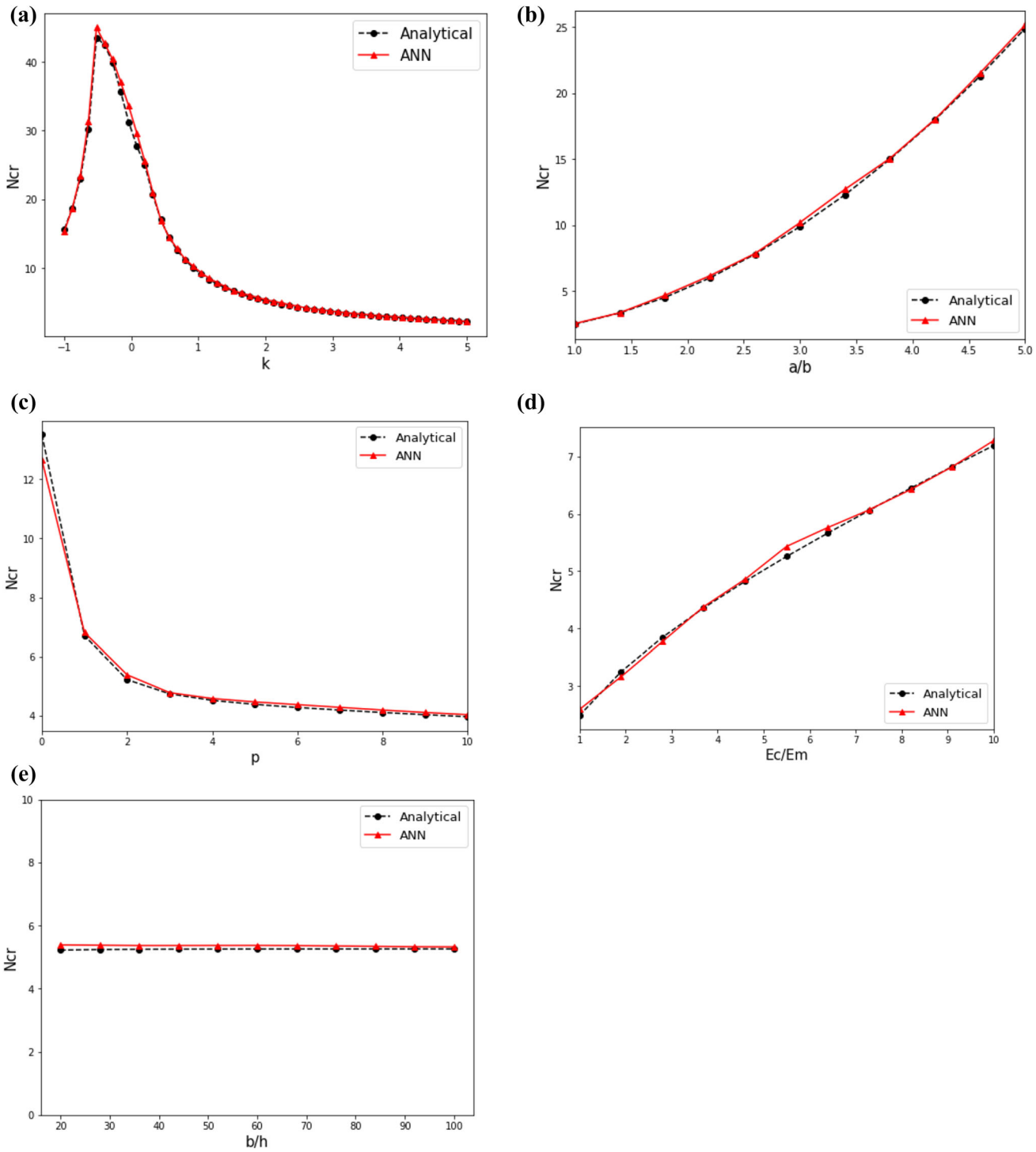

Fig. 7 The effect on nondimensional critical buckling load of FG rectangular plate under biaxial compression: **a** biaxial compression factor (k); **b** aspects ratio (a/b); **c** volume fraction exponent (p); **d** material component ratio (Ec/Em); **e** thickness ratio (b/h)

used to indicate standard deviation, coefficient of variance, and mean of the parameters, respectively. The subscripts of these symbols (e.g., $\sigma_{a/b}$, $CV_{a/b}$ and $\mu_{a/b}$) refer to corresponding variables.

The effects of the various geometric and material parameters on the mean of $\overline{N}_{cr}$ are examined using the database obtained from the MCS. The distribution of the mean of $\overline{N}_{cr}$ against the variations of the mean of input

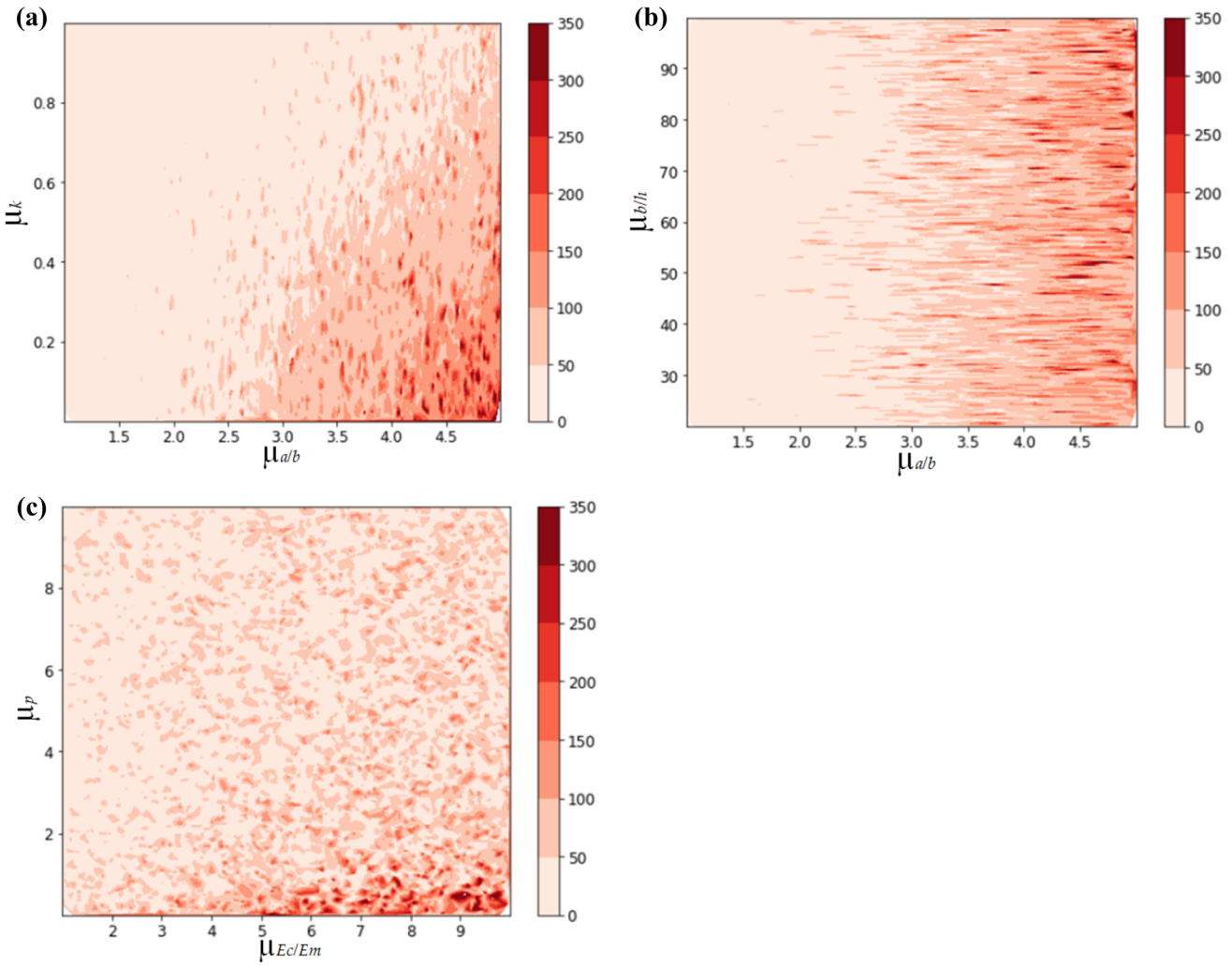

Fig. 8 Contour map of mean of $\overline{N}_{\mathrm{cr}}$ versus mean of: **a** aspect ratio and loading coefficient (i.e., $\mu_{a/b}$ and μ_k); **b** geometric parameters (i.e., $\mu_{\mathrm{a/b}}$ and $\mu_{b/h}$); **c** material parameters (i.e., $\mu_{Ec/Em}$ and μ_p)

variables is plotted in Fig. 8. The figure plots a contour map of the mean of $\overline{N}_{\mathrm{cr}}$ for two input variables on the *x*- and *y*-axes, respectively. The darker color in the figure corresponds to a higher mean of $\overline{N}_{\mathrm{cr}}$.

Figure 8a shows the contour map for $\mu_{a/b}$ and μ_k, where the darker color is concentrated near to the lower right corner. Thus, the higher mean of $\overline{N}_{\mathrm{cr}}$ is correlated with higher $\mu_{a/b}$. The highest buckling loads are concentrated in the region with $a/b > 2.5$. The buckling load also depends on *k*, with the high values of $\mu_{\overline{N}_{\mathrm{cr}}}$ (i.e., larger than 100) concentrated in the lower right corner. The distribution of color is nearly uniform along the vertical axis in Fig. 8b, indicating insignificant effects of $\mu_{b/h}$ on $\mu_{\overline{N}_{\mathrm{cr}}}$, while the critical buckling load of the plate is higher with higher $\mu_{a/b}$ (as in Fig. 8a). The contour map with μ_p and $\mu_{Ec/Em}$ in Fig. 8c shows a weak concentration of dark color near the lower right corner. This figure indicates a relatively weaker correlation of high $\mu_{\overline{N}_{\mathrm{cr}}}$ with μ_p. The $\mu_{\overline{N}_{\mathrm{cr}}}$ is apparently higher for higher $\mu_{Ec/Em}$ and lower μ_p. Similar effects of standard deviations of the input parameters on the standard deviation of $\overline{N}_{\mathrm{cr}}$ are observed (but not included in the paper for the sake of brevity).

The correlations of the mean and standard deviations of the input variables with the mean and standard deviation of $\overline{N}_{\mathrm{cr}}$ are examined, as shown in Fig. 9. It shows that the $\mu_{\mathrm{a/b}}$ has a significant correlation with $\mu_{\overline{N}_{\mathrm{cr}}}$ and $\sigma_{\overline{N}_{\mathrm{cr}}}$ with the correlation coefficients of 0.6538 and 0.5799, respectively. The $\sigma_{b/a}$ has the strongest correlation to $\sigma_{\overline{N}_{\mathrm{cr}}}$ with the correlation coefficient of 0.6764. The input *k* has the most negative correlation to $\overline{N}_{\mathrm{cr}}$ with the correlation coefficients of -0.3906 and -0.2761 for $\mu_{\overline{N}_{\mathrm{cr}}}$ and $\sigma_{\overline{N}_{\mathrm{cr}}}$, respectively. The *p* has a negative effect on $\overline{N}_{\mathrm{cr}}$ while *a/b* and E_c/E_m

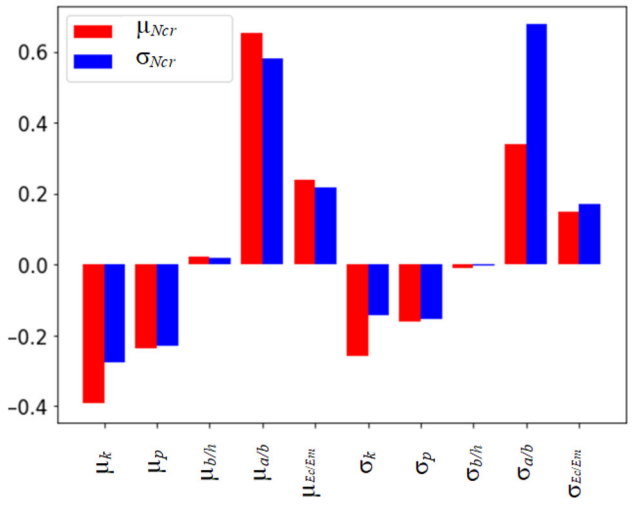

Fig. 9 Correlation coefficients of $\mu_{\overline{N}_{cr}}$ and $\sigma_{\overline{N}_{cr}}$

have positive effects $\overline{N}_{cr}$ (similar to those observed in Fig. 8).

The effects of CVs of inputs on the CV_ $\overline{N}_{cr}$ are examined in Fig. 10, where the variations of the buckling load are plotted against the variations of random variables. The figure presents the results for cases with $\mu_{Ec/Em}$ = 380/70; μ_p = 2; $\mu_{b/h}$ = 20; $\mu_{a/b}$ = 2; and μ_k = 1. For the effects of each variable, the CV for the other variables is set at zero (the variables are set to constant values). Thus, one random variable is changed at a time. As seen in the figure, $CV_{\overline{N}_{cr}}$ generally increases with the increase in the CVs of the random variables. However, the magnitudes of the changes depend on the mean values of the input parameters and their importance levels to the $\overline{N}_{cr}$. As expected, $CV_{\overline{N}_{cr}}$ increases more significantly for the more important input parameters, such as a/b (Fig. 10b). For all other parameters, the variation in the output ($\overline{N}_{cr}$) is less (i.e., < 0.2) than the variation of the input parameters (i.e., 0.2). The effect of uncertainty in *b/h* appears to be the lowest, and insignificant with the maximum $CV_{\overline{N}_{cr}}$ of 0.0041 (for $\mu_{b/h}$ = 80 and $CV_{b/h}$ = 0.2), shown in Fig. 10e.

Figure 10 also shows that $CV_{\overline{N}_{cr}}$ consistently increases with the increase in means of *k* and *a/b* (Fig. 10a, b). For *p*, and E_c/E_m, the $CV_{\overline{N}_{cr}}$ initially increases with the increase in mean values of the parameter and then decreases. For example, $CV_{\overline{N}_{cr}}$ increases by increasing the μ_p from 0.2 to 1, and then decreases with further increase in the μ_p to 5 (Fig. 10c). Among different parameters, the uncertainties in *b/a* are found to have the most significant effect on $\overline{N}_{cr}$, followed by *k* and E_c/E_m.

4 Conclusions

In this paper, an ANN model is developed for the assessment of the critical buckling load of simply supported FGM plates. The data for the development of ANN model were generated through an analytical solution obtained based on the first-order shear deformation theory. A major limitation of the analytical solution is that it is too complex to apply in engineering practice and requires trials to solve equations for various modes to obtain the minimum load as the critical buckling load. This limitation could be overcome using the proposed ANN model, which provides a simplified solution for the complex engineering problems of FMG plates. The model developed for the simply supported FGM plates includes six input variables, representing the biaxial load factor, the geometrical parameters, and the material properties. A network with six hidden layers with each layer of 32 nodes (plus 1 bias node) leads to the successful development of the ANN model with a coefficient of determination of around 99.95%.

Among the different parameters, biaxial compression factor k is found to have the most significant effect on the nondimensional critical buckling load. The critical buckling load is the highest for a tensile load of 50% of the compression load along the orthogonal direction (k =— 0.5). The critical buckling load decreases with a further increase in tensile load and compression load toward the orthogonal direction. The critical buckling load increases with the increase in *a/b* and *Ec/Em* and decreases with the increase in *p*. The length to thickness ratio, *b/h*, has an insignificant effect on the critical buckling load, $\overline{N}_{cr}$.

The first- and second-order stochastic characteristics of $\overline{N}_{cr}$ have been examined based on the results of 10^6 MCSs. The mean values of the inputs are chosen as the normally distributed random variables, while the coefficients of variance are uniformly distributed within [0:0.2]. Among the different parameters, *a/b* and *k* are found to influence the statistical characteristics of $\overline{N}_{cr}$ most significantly. The critical buckling load increases with the increase in *a/b* and E_c/E_m and decreases with the increase in *p* and *k*.

The $CV_{\overline{N}_{cr}}$ is found to increase almost linearly with the increase in the CVs of the input variables. The critical buckling loads are more sensitive to the variations of the mean values of the input parameters. The variation in the critical buckling load ($CV_{\overline{N}_{cr}}$) can be greater than the variation in b/a (i.e., $CV_{b/a}$) while $CV_{\overline{N}_{cr}}$ is less than the coefficient of variance of the other parameters.

The ANN model presented here provides a surrogate to the computationally expensive finite element analysis and iterative analytical solution of the complex buckling problem of FGM plates. The simplified model is useful for

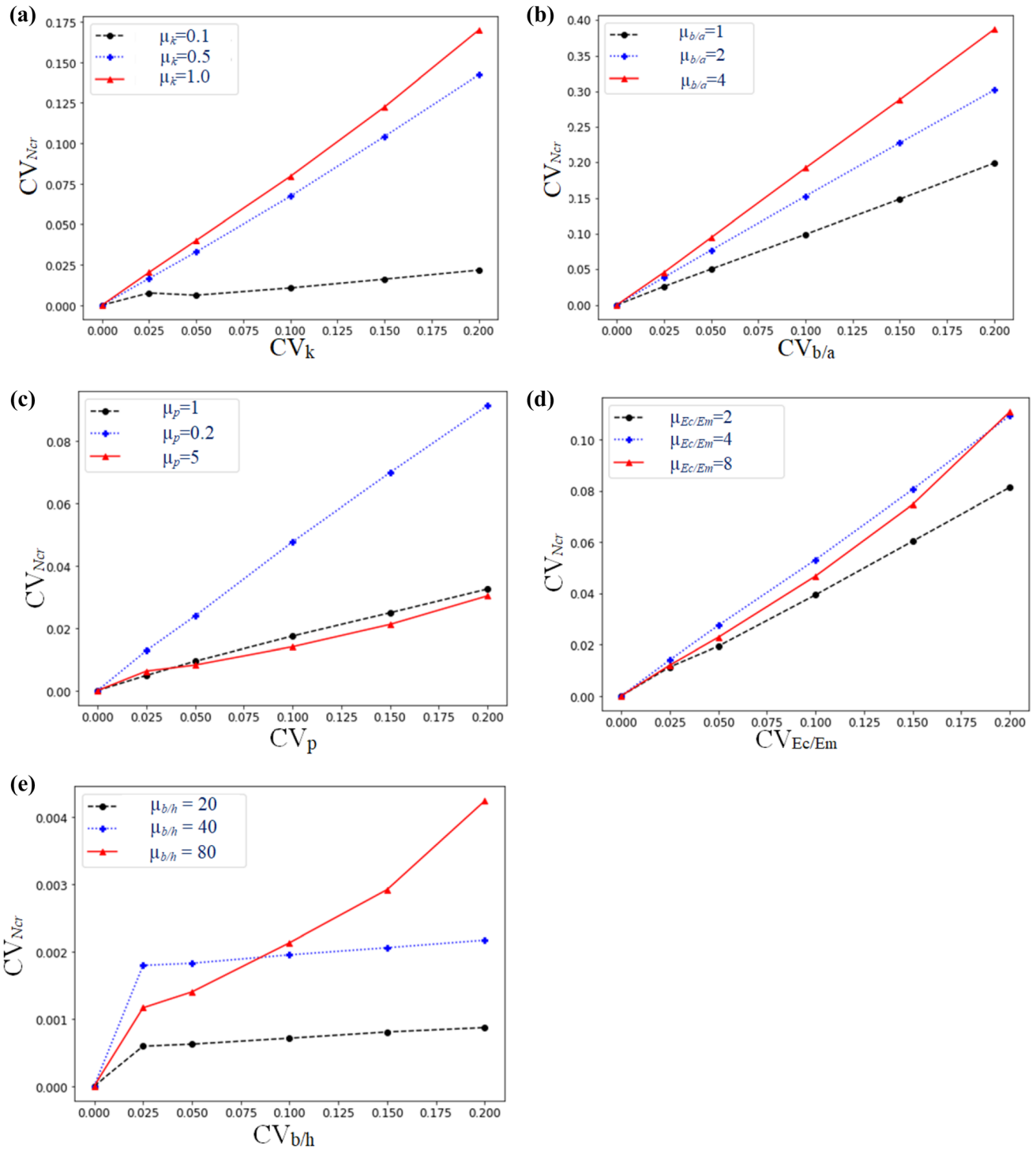

Fig. 10 Effect of randomness of input parameters on critical buckling load: **a** biaxial compression factor; **b** aspects ratio; **c** volume fraction exponent; **d** material component ratio; **e** thickness ratio

studying the uncertainties of the critical buckling load due to variabilities in the input parameters using statistical analysis. Future work will involve improving the model to cover a wide range of edge constraints and geometries (i.e., circular or quadrilateral) of the plates. The proposed method can be used to develop ANN models for other complex structural problems.

Funding This research was funded by ARES-CCD (Académie de Recherche et d'Enseignement supérieur - Commission de la

Coopération au Développement) in the framework of the Institutional Support to Vietnam National University of Agriculture (VNUA).

Data availability The data required to reproduce these findings will be made available on request.

Declarations

Conflicts of interest The authors declare no conflict of interest.

References

1. Zhao X, Lee Y, Liew KM (2009) Mechanical and thermal buckling analysis of functionally graded plates. Compos Struct 90(2):161–171
2. Bodaghi M, Saidi A (2010) Levy-type solution for buckling analysis of thick functionally graded rectangular plates based on the higher-order shear deformation plate theory. Appl Math Model 34(11):3659–3673
3. Shariat BS, Eslami M (2007) Buckling of thick functionally graded plates under mechanical and thermal loads. Compos Struct 78(3):433–439
4. Thai H-T, Choi D-H (2012) An efficient and simple refined theory for buckling analysis of functionally graded plates. Appl Math Model 36(3):1008–1022
5. Thai H-T, Kim S-E (2013) Closed-form solution for buckling analysis of thick functionally graded plates on elastic foundation. Int J Mech Sci 75:34–44
6. Thai H-T, Choi D-H (2013) Analytical solutions of refined plate theory for bending, buckling and vibration analyses of thick plates. Appl Math Model 37(18–19):8310–8323
7. Thai H-T, Vo TP (2013) A new sinusoidal shear deformation theory for bending, buckling, and vibration of functionally graded plates. Appl Math Model 37(5):3269–3281
8. Nguyen T-K, Vo TP, Thai H-T (2014) Vibration and buckling analysis of functionally graded sandwich plates with improved transverse shear stiffness based on the first-order shear deformation theory. Proc Inst Mech Eng C J Mech Eng Sci 228(12):2110–2131
9. Van Tung H, Duc ND (2010) Nonlinear analysis of stability for functionally graded plates under mechanical and thermal loads. Compos Struct 92(5):1184–1191
10. Huan DT, Tu TM, Quoc TH (2017) Analytical solutions for bending, buckling and vibration analysis of functionally graded cylindrical panel. Vietnam J Sci Technol 55(5):587
11. Tran M-T et al (2020) Free vibration of stiffened functionally graded circular cylindrical shell resting on Winkler–Pasternak foundation with different boundary conditions under thermal environment. Acta Mech 231(6):2545–2564
12. Thinh TI et al (2016) Vibration and buckling analysis of functionally graded plates using new eight-unknown higher order shear deformation theory. Lat. Am. J. solids struct. 13(3):456–477
13. Tu TM et al (2017) Bending analysis of functionally graded plates using new eight-unknown higher order shear deformation theory 62(3):311–324
14. Van Long N, Quoc TH, Tu TMJ (2016) Bending and free vibration analysis of functionally graded plates using new eight-unknown shear deformation theory by finite-element method. Int J Adv Struct Eng. 8(4):391–399
15. Belabed Z et al (2014) An efficient and simple higher order shear and normal deformation theory for functionally graded material (FGM) plates. Compos B Eng 60:274–283
16. Yang J, Liew K, Kitipornchai S (2005) Second-order statistics of the elastic buckling of functionally graded rectangular plates. Compos Sci Technol 65(7–8):1165–1175
17. McCulloch WS, Pitts W (1943) A logical calculus of the ideas immanent in nervous activity. Bull Math Biophys 5(4):115–133
18. LeCun Y, Bengio Y (1995) Convolutional networks for images, speech, and time series. The handbook of brain theory and neural networks 3361(10):1995
19. Carreira-Perpinan MA, Hinton GE (2005) On contrastive divergence learning. in Aistats. Citeseer.
20. Hinton GE, Osindero S, Teh Y-W (2006) A fast learning algorithm for deep belief nets. Neural Comput 18(7):1527–1554
21. Ranzato MA et al (2007) Unsupervised learning of invariant feature hierarchies with applications to object recognition. In: 2007 IEEE conference on computer vision and pattern recognition. IEEE
22. Duong HT et al (2020) Optimization design of rectangular concrete-filled steel tube short columns with balancing composite motion optimization and data-driven model. In: Structures. Elsevier
23. Le T-T (2021) Prediction of tensile strength of polymer carbon nanotube composites using practical machine learning method. J Compos Mater 55(6):787–811
24. Le T-T, Phan HC (2020) Prediction of ultimate load of rectangular CFST columns using interpretable machine learning method. Adv Civ Eng 2020:8855069
25. Oh D et al (2020) Burst pressure prediction of API 5L X-grade dented pipelines using deep neural network. J Mar Sci Eng 8(10):766
26. Phan HC, Duong HT (2021) Predicting burst pressure of defected pipeline with principal component analysis and adaptive neuro fuzzy inference system. Int J Pressure Vessels Piping 189:104274
27. Ootao Y, Tanigawa Y, Nakamura T (1999) Optimization of material composition of FGM hollow circular cylinder under thermal loading: a neural network approach. Compos B Eng 30(4):415–422
28. Liu G et al (2001) Material characterization of functionally graded material by means of elastic waves and a progressive-learning neural network. Compos Sci Technol 61(10):1401–1411
29. Jodaei A, Jalal M, Yas M (2012) Free vibration analysis of functionally graded annular plates by state-space based differential quadrature method and comparative modeling by ANN. Compos B Eng 43(2):340–353
30. Han X, Xu D, Liu G-R (2003) A computational inverse technique for material characterization of a functionally graded cylinder using a progressive neural network. Neurocomputing 51:341–360
31. Nazari A, Milani AA, Zakeri M (2011) Modeling ductile to brittle transition temperature of functionally graded steels by artificial neural networks. Comput Mater Sci 50(7):2028–2037
32. Reddy J (2000) Analysis of functionally graded plates. Int J Numer Meth Eng 47(1–3):663–684
33. Yin S et al (2014) Isogeometric locking-free plate element: a simple first order shear deformation theory for functionally graded plates. Compos Struct 118:121–138
34. Hosseini-Hashemi S et al (2010) Free vibration of functionally graded rectangular plates using first-order shear deformation plate theory. Appl Math Model 34(5):1276–1291
35. Thai H-T, Choi D-H (2013) Size-dependent functionally graded Kirchhoff and Mindlin plate models based on a modified couple stress theory. Compos Struct 95:142–153
36. Reddy JN (2006) Theory and analysis of elastic plates and shells. CRC Press, Boca Raton
37. Rumelhart DE, Hinton GE, Williams RJ, Learning internal representations by error propagation. 1985, California Univ San Diego La Jolla Inst for Cognitive Science

38. Phan HC, Dhar AS (2021) Predicting pipeline burst pressures with machine learning models. Int J Pressure Vessels Piping, 2021
39. Ho TK (1995) Random decision forests. In: Proceedings of 3rd international conference on document analysis and recognition. IEEE
40. Ho TK (1998) The random subspace method for constructing decision forests. IEEE Trans Pattern Anal Mach Intell 20(8):832–844
41. Friedman JH (2001) Greedy function approximation: a gradient boosting machine. Ann Stat 29:1189–1232
42. Boser BE, Guyon IM, Vapnik VN (1992) A training algorithm for optimal margin classifiers. In: Proceedings of the fifth annual workshop on computational learning theory
43. Cortes C, Vapnik V (1995) Support-vector networks. Mach Learn 20(3):273–297
44. Vapnik V (1998) Statistical learning theory. Wiley, New York